AIAA SciTech Forum
23-27 January 2023, National Harbor, MD & Online
AIAA SCITECH 2023 Forum

10.2514/6.2023-2337

Tagging Velocimetry in the Stevens Shock Tunnel

B. A. Segall*, D. Shekhtman†, A. Hameed‡, J. H. Chen§, and N. J. Parziale¶
Stevens Institute of Technology, Hoboken, NJ 07030, USA

Tagging velocimetry is demonstrated in the Stevens Shock Tunnel to obtain velocity profiles in high-speed flows over a hollow-cylinder-flare test article. Acetone was used as the tagged tracer in shock-tunnel-generated high-speed air flow, excited by the fourth harmonic of the burst-mode Nd:Yag laser (266 nm) at 50 kHz. Freestream velocity is recorded and matches predicted values with good agreement. Additionally, turbulent boundary layer velocity profiles are reported.

I. Introduction

Tagging velocimetry serves as a nonintrusive diagnostic technique in the hypersonic flow regime, providing off-surface, time-of-flight velocity profile measurements. By using high repetition lasers and high-speed camera imaging, it can interrogate freestream flows and flows over canonical geometries in ground-test facilities. Time-resolved velocimetry data can then be used to verify tunnel functionality, quantify turbulence quantities, and describe unsteady boundary layer profiles. Designers of hypersonic vehicles can use tagging velocimetry results to verify computational fluid dynamic (CFD) predictions of flow structures and visualize flow profiles over test articles in regions where CFD encounters difficulty, such as separation bubbles [1].

Several popular tracers used for tagging velocimetry include krypton [2–11], oxygen [12], acetone [13, 14], biacetyl [15], hydroxyl [16–19], iodine [20, 21], nitric oxide [22], nitrogen [23–26], and argon [27] as well as many others.

The molecular tracer, acetone, has become quite popular in recent studies. Acetone tagging at 266 nm was demonstrated by Lempert et al. [13, 14] in an acetone-seeded nitrogen free jet with a 250-500 ns interframe time and a camera gate of 20 ns. Images were averaged over 3-10 s at a repetition rate of 10 Hz. Gragston et al. [28] performed acetone tagging at 10 kHz in acetone-seeded air to probe the freestream and the turbulent boundary layer of the test section of the UTSI Mach 4 Ludwieg Tube. Gating and interframe times are not reported. Andrade et al. [29]) performed 10 kHz acetone tagging of acetone-seeded nitrogen gas flows in the freestream and test section wall of the UT Mach 7 Ludwieg Tube Wind Tunnel, using a gate of 1 µs and an interframe time of approximately 10 microseconds.

Acetone is readily available and inexpensive and the excitation spectrum of acetone is accessible by the fourth harmonic of an Nd:Yag laser (266 nm) [30, 31]. There exists ambiguity in our understanding of the photophysics and lifetime of acetone in laser-induced fluorescence and phosphorescence experiments. Lempert et al. [13, 14] report a signal lifetime of less than 500 ns, which justifies their interframe time delay of 230 ns. Tran [32] and Lozano [30] both note that phosphorescence of acetone is heavily quenched by small quantities of oxygen. The phosphorescence lifetime of oxygen-free acetone vapor is 200 µs [32], and the presence of minute quantities of oxygen greatly reduces its lifetime [33, 34]. Yet, Gragston et al. [28] report lifetimes on the order of microseconds for acetone-seeded air. Fratantonio et al. [31] state that the optimal excitation wavelength for phosphorescence in acetone is at 308 nm with a lifetime of 50 µs. In contrast to reseachers using the phosphorescence of acetone, we follow the approach of Lempert et al. [13, 14] utilizing acetone fluorescence.

Ultimately, this work aims to make mean-velocity profile measurements of a hypersonic, turbulent boundary layer on a hollow-cylinder flare (HCF) in the Stevens Shock Tunnel using a high-repetition-rate laser and a high-speed camera for time-resolved velocity profiles.

II. Experimental Setup

A. Ground-Test Facility Facility

The Stevens Shock Tunnel is a facility designed to replicate Mach 6 free-flight flow conditions with an enthalpy of 1.5 MJ/kg and a unit Reynolds number 0.35 - 8.1 $\times$ 10^6 m^{-1} for at least 5 ms when using helium as a driver gas. The construction of the shock tunnel adheres to ASME standard B16.5 Pipe Flanges and Flanged Fittings for flanges and olets [35] and ASME standard B31.1 Power Piping for all pipes [36]. In Fig. 1, the current configuration of the tunnel is displayed. The driver section is 5.0 m long, and the driven section is 11.07 m long. A double diaphragm is used to start the tunnel. Up to 5 transducer stations are used to provide a shock-speed measurement. The test section has an inner diameter of 0.610 m (24 in) and is large enough to accommodate a 34° hollow-cylinder flare of 0.102 m (4 in) outer cylinder diameter and 0.203 m (8 in) outer flare diameter without tunnel startup issues. A Pitot pressure probe is located at the nozzle exit in order to determine freestream conditions during each run, via the Rayleigh-Pitot tube relation and the assumption of isentropic nozzle flow [3, 37]. Further mechanical details on the Stevens Shock Tunnel can be found in [38].

The tunnel runs were conducted with nitrogen N_2 as the driver gas. Acetone vapor was seeded into the driven-section test gas via a bubbler. A graduated cylinder was used to measure the volume of liquid acetone before and after the filling process to determine the mass of acetone vapor in the driven gas. A fixed-point iteration method using Cantera [39] was used to calculate the mole fraction of acetone in the test gas. Run conditions are shown in Table 1. Reservoir conditions were calculated with both Cantera and the Shock and Detonation Toolbox [40]. The appropriate thermodynamic data are found in the literature [41, 42]. Freestream conditions were calculated via the method described in Mustafa et al. [6], utilizing reservoir and Pitot pressure traces and assuming an isentropic expansion iterating to find freestream Mach number. Representative pressure traces for shots 270 through 272 are shown in Figs. 3a to 3c. With nitrogen gas as the driver, test times of up to 10 ms can be achieved, limited by the arrival of a compression wave, which is generated by the reflection of the reflected shock at the contact surface. With the use of a diaphragm debris blocker, as described in [38], the Pitot traces exhibit small oscillation and demonstrate the establishment of steady flow during test times indicated by a heavy red lineweight.

Using nitrogen as the driver gas and a pressure ratio of 10, typical enthalpy in the nozzle reservoir is 0.5 MJ/kg. At a steady state temperature exceeding 573 K [43], acetone will pyrolyze in the nozzle reservoir, reducing tracer signal. More specifically, according to Capelin et al. [44], acetone will pyrolyze noticeably at 650 K and completely by 850 K. However, the danger of acetone pyrolysis is reduced considerably by the short run times of the tunnel ($\approx$ 20 ms), as a result of a kinetics study, shown in Fig. 2, using reaction mechanism modelling from Yu et al. [45]. For temperatures below 1200 K for acetone-seeded nitrogen and air at pressure 3.5 MPa, there is no observed acetone decomposition during the useful test time of the Stevens Shock Tunnel. Therefore, acetone-seeded air can be used for shock tunnel

*Graduate Student, Mechanical Engineering, Castle Point on Hudson, Hoboken, New Jersey, 07030.
†Postdoctoral Researcher, Mechanical Engineering, Castle Point on Hudson, Hoboken, New Jersey, 07030.
‡Graduate Student, Mechanical Engineering, Castle Point on Hudson, Hoboken, New Jersey, 07030.
§Graduate Student, Mechanical Engineering, Castle Point on Hudson, Hoboken, New Jersey, 07030.
¶Associate Professor, Mechanical Engineering, Castle Point on Hudson, Hoboken, New Jersey, 07030, AIAA Associate Fellow.

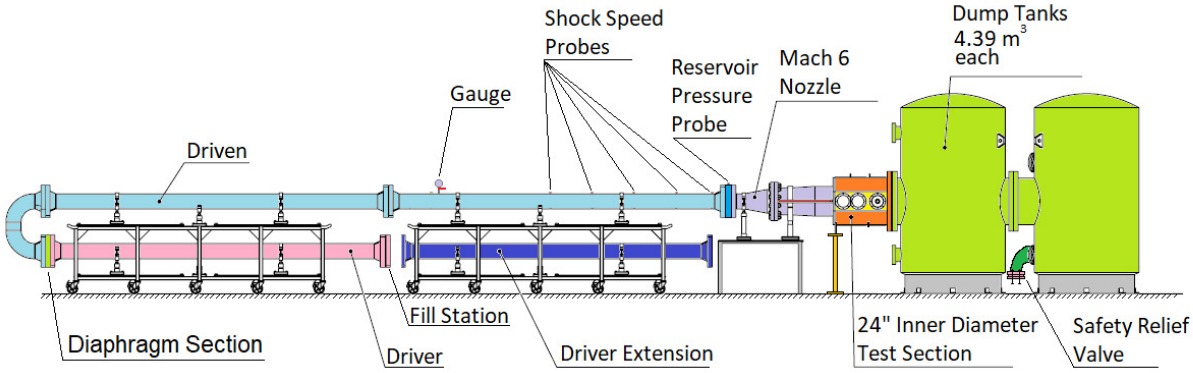

Fig. 1 Schematic of Stevens Shock Tunnel.

experiments in which the nozzle reservoir does not exceed 1200 K and a pressure of 3.5 MPa (500 psi), such that the timescale of acetone pyrolysis is less than that of the tunnel test time, which is the case for 1% acetone/99% air gas mixture.

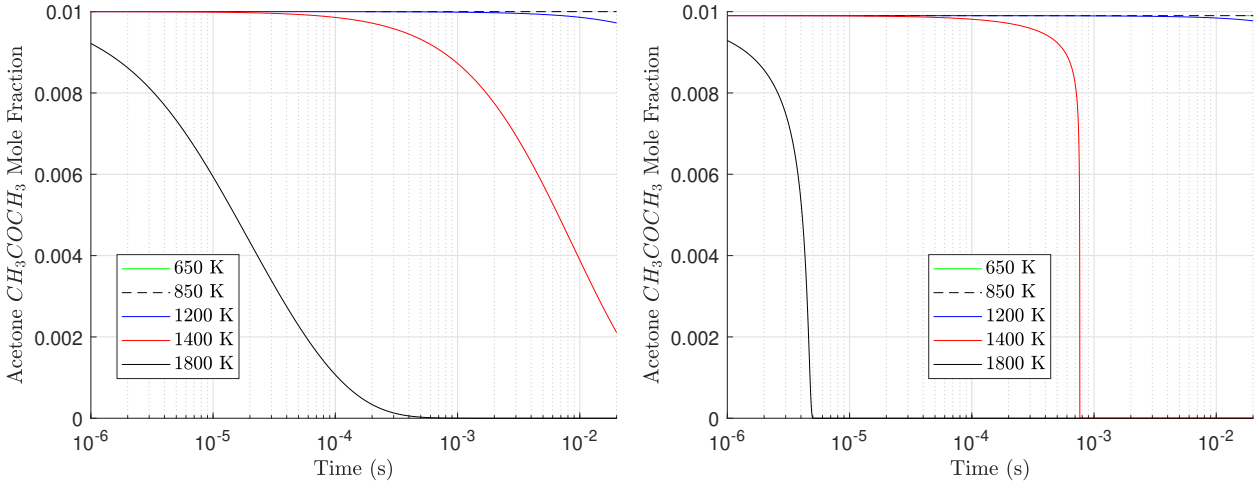

(a) Nitrogen **(b) Air**

Fig. 2 Acetone Mole Fraction vs. Time in seeded Nitrogen (a) and Air (b).

Table 1 Run Conditions, where P_4 is Driver-section nitrogen gas pressure; P_4/P_1 is the driver-to-driven pressure ratio that determines the driven air gas pressure P_1; u_s is the shock speed; M_s is the shock Mach number; T_r is the reservoir temperature; P_r is the reservoir pressure; P_∞ is the freestream pressure, T_∞ is the freestream temperature, M_∞ is the freestream Mach number, V_∞ is the time-averaged freestream velocity, and Re^u_∞ is the unit Reynolds number. Freestream pressure, temperature, velocity, and Reynolds number are calculated nozzle pitot tube and nozzle reservoir pressures, using the method described in Mustafa et al. [6], assuming an isotropic nozzle with chemical reactions.

Shot	P_4 (MPa)	$\frac{P_4}{P_1}$	$X_{C_3H_6O}$	u_s (m/s)	M_s	P_R (MPa)	T_r (K)	P_∞ (kPa)	T_∞ (K)	M_∞	V_∞ (m/s)	Re^u_∞ (10^6 1/m)
270	3.44	10	0.0088	504	1.46	1.76	485	1.01	58.7	6.07	935	14.7
271	1.06	10	0.0087	527	1.53	0.65	515	0.368	62.0	6.09	964	4.88
272	1.76	10	0.0087	527	1.53	1.08	516	0.611	62.2	6.09	966	8.08
274	3.46	10	0.023	505	1.48	2.48	505	1.25	62.9	6.02	960	16.0
276	3.46	10	0.0079	528	1.52	2.11	516	1.25	62.9	6.04	964	16.1

B. Experimental Tagging Velocimetry Setup

As shown in Fig. 4, acetone tagging experiments in the tunnel freestream utilized an externally triggered Spectral Energies QuasiModo Burst-Mode Laser System, set at 40 kHz CW - 5.5 ms with a 4 ms burst train duration and a repetition rate of 50 kHz. The average pulse train energy was 7.75 J for 200 pulses, resulting in an average pulse energy of ≈38 mJ. During a test run, the start of the pulse burst train was triggered by the rising edge of a reservoir pressure transducer. At a set delay (7.0 ms) from this rising edge, the burst-mode laser system pulses for 4.0 ms at the excitation wavelength into the test section. For acetone tagging, the fourth harmonic of the Nd:Yag laser, 266 nm, was selected based on the work of Lozano [30]. The pulse is directed towards the test section and is focused by an f = 500 mm plano-convex lens. The beam enters the test section through a 0.0254 m (1 in) diameter, 3 mm (0.12 in) thick fused-silica glass window.

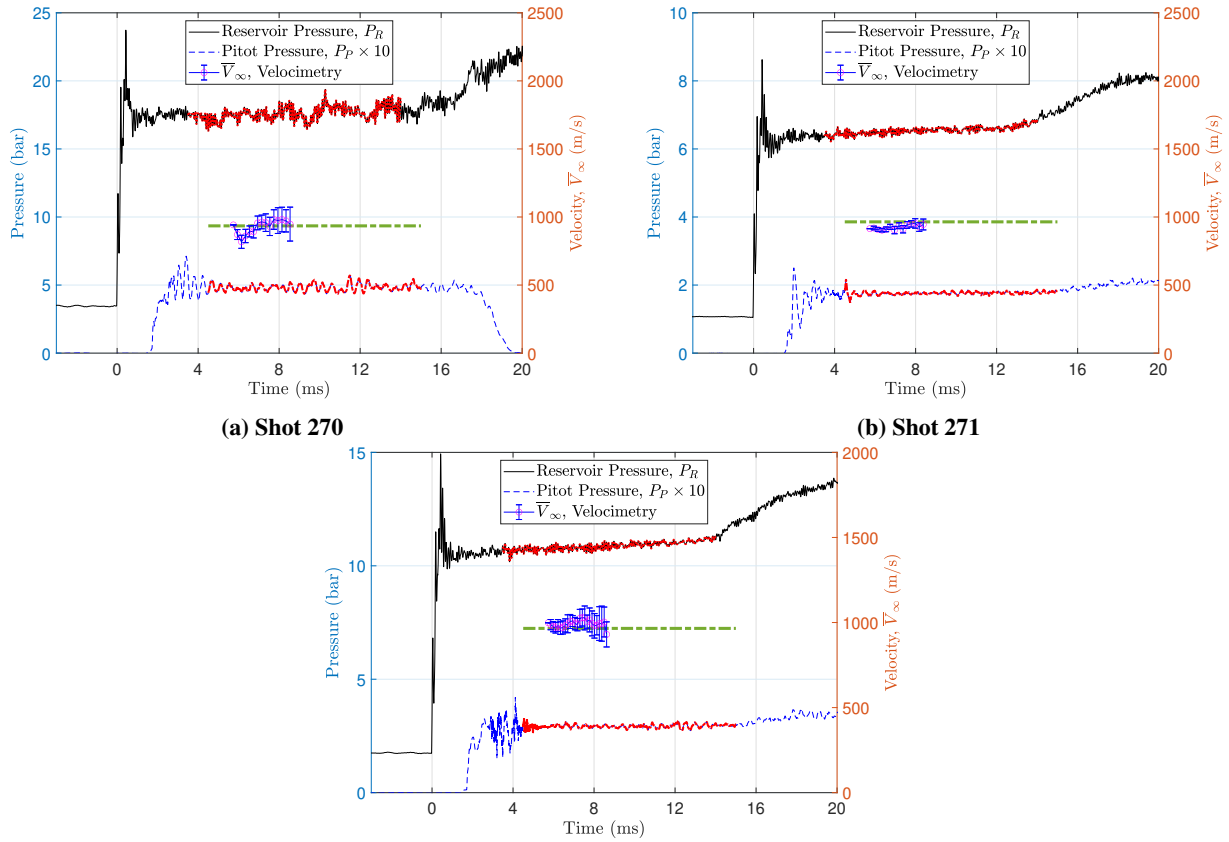

(a) Shot 270

(b) Shot 271

(c) Shot 272

Fig. 3 Pressure Traces and Freestream Velocimetry Data for Stevens Shock Tunnel Experiments. Test times are indicated by a thick red lineweight. Run conditions are listed in Table 1.

The approach and coordinate transformation of Mustafa et al. [10] were implemented to interrogate the boundary layer. As shown in Fig. 5, the 266 nm excitation laser beam was oriented approximately tangential to the hollow cylinder portion of the test article, in a location outside the flare interaction region. Additionally, to increase wall resolution, the beam was focused to ≈33 µm near the true tangent of the cylinder. By grazing the surface of the cylinder, the size of the laser-induced ablation plume at the wall was minimized. The probing location was 0.9 m (35.5 in) from the cylinder leading edge. A 0.15 m (6 in) long trip composed of 40 grit and 50 grit sanding belts was placed 0.26 m (10 in) from the sharp leading edge to trip turbulence. A coordinate transformation between the measured image coordinate y_m from the no-slip condition to the wall-normal coordinate y was derived, using Fig. 5 and the Pythagorean Theorem:

$$y = \sqrt{\left(R\cos\left(\sin^{-1}\frac{y_w}{R}\right)\right)^2 + (y_m + y_w)^2} - R, \tag{1}$$

where R is the radius of the hollow cylinder (0.0508 m) and y_w is the location of the no-slip condition from the true tangent of the cylinder, as seen by the camera. Eq. 1 simplifies to

$$y = \sqrt{R^2 + y_m^2 + 2y_m y_w} - R. \tag{2}$$

The imaging system consisted of a Phantom TMX 7510 with a 135 mm Carl Zeiss lens. The length scale is 15.0 pixels/mm. The gate width of the Phantom camera was set to 100 ns. The camera was pulsed by a Berkeley Nucleonics Model 577 pulse generator, which was triggered at 50 kHz by the QuasiModo Quantum Composer (a signal generator inside the laser), resulting in a frame rate of 50 kHz (20 µs between frames). The Model 577 pulse generator synchronized the camera strobe (gate). Using its duty-cycle feature, the pulse generator timed the capture of the write image at user-defined locations within a given pulse train. It would wait a set number of pulses before obtaining a write

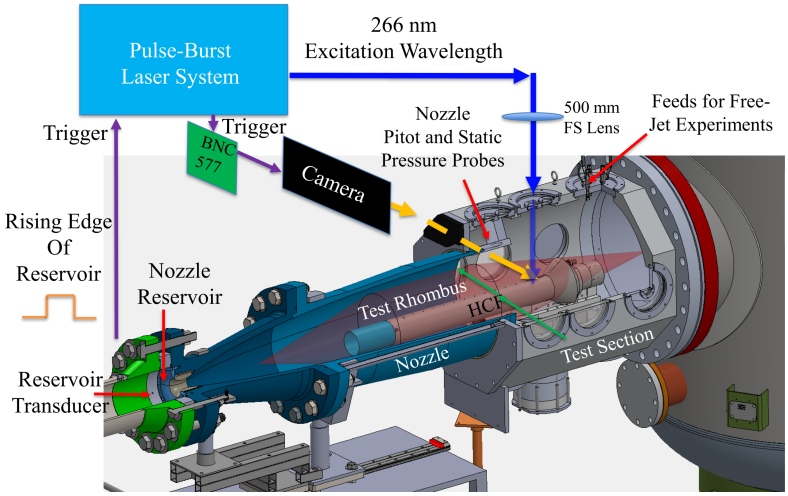

Fig. 4 Experimental Setup for Tagging Velocimetry in the Stevens Shock Tunnel.

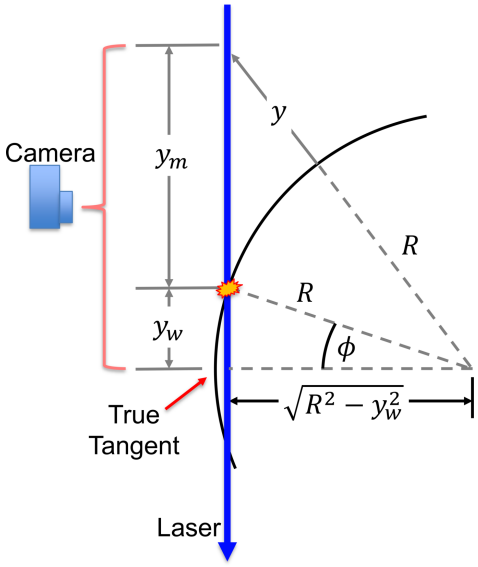

Fig. 5 Schematic that geometrically relates the image coordinate y_m to wall-normal coordinate y.

image. Within this set number, read images would be captured. For the experiments in this work, a write frame was generated every 11 frames.

III. Shock Tunnel Results

Acetone tagging results are presented below for shock tunnel experiments, whose run conditions are listed in Table 1. Typical acetone mole fractions less 1% were used. A write-read interframe time of 450 ns was used to allow sufficient displacement to capture signal, observe structure, and minimize velocity measurement error. Shot 272 however used an interframe time of 700 ns. Sample processed images are shown in Fig. 6. Images were (1) smoothed via a Wiener Filter, (2) lowpass filtered with a Fast Fourier Transform disc filter, and (3) processed via the peak finding algorithm of O'Haver [46], which fits a Gaussian to the peak of each row. In Fig. 7a, over 100 profiles are plotted. In Fig. 7b, average velocity profiles are plotted for the five shock tunnel experiments listed in Table 1. The coordinate transformation, Eq. 2, effectively stretched the turbulent boundary layer, potentially capturing the log law and viscous sublayer regions. Future work will involve further reducing this data and confirming the efficacy of the data very close to the wall.

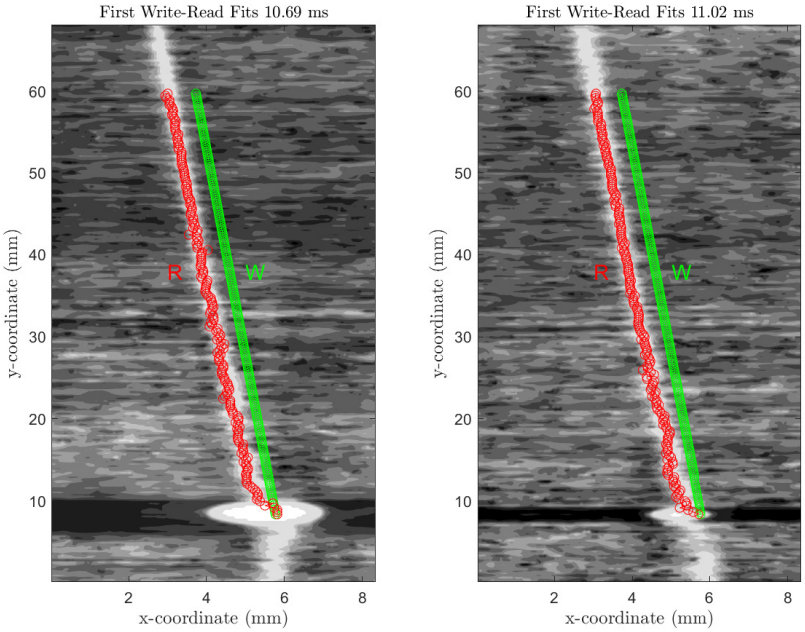

Fig. 6 Representative Write-and-read Frame Fitting at 5 frames after Each Write Frame in Shot 272. The letters W and R indicate a write fit and a read fit, respectively.

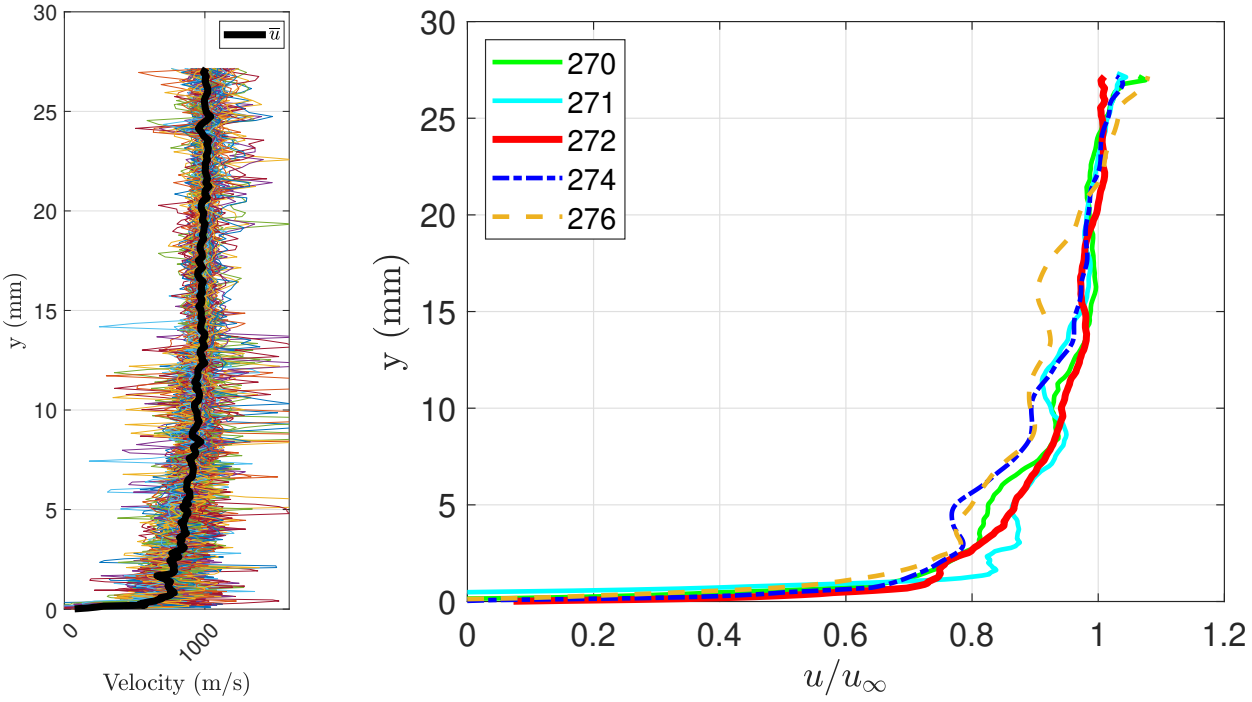

(a) Shot 272 Profiles **(b) Average Profiles**

Fig. 7 Turbulent Profiles obtained via Acetone Tagging. (a) Profiles for individual read frames for Shot 272. The heavy Black line represent $\overline{u}$. (b) Average Velocity Profiles for shock tunnel experiments.

IV. Conclusion

Acetone tagging at nominally 1 % mole fraction was conducted in nitrogen-driven shock-tunnel-generated acetone-seeded air flows at Mach 6. Tagging results over a hollow cylinder flare are presented for five experiments. Measured freestream velocities show good agreement with velocity, calculated by our freestream solver. We believe that, in a turbulent boundary layer, the no-slip condition was observed, and near-wall resolution was established. As such, the viscous sublayer and log law regions of a turbulent boundary layer were potentially resolved. The intensity of the acetone tracer can be potentially used to obtain the density profile of the turbulent boundary layer. Additional work towards conducting Krypton tagging velocimetry with a burst-mode OPO is ongoing in order to reduce required laser energy and guarantee inertness of the tagged tracer.

Acknowledgments

Ben A. Segall, David Shekhtman, Ahsan Hameed, James H. Chen, and Nicholaus J. Pariale were supported by ONR and AFOSR Grants, including N00014-19-1-2523, N00014-20-1-2637, N00014-20-1-2549, FA9550-16-1-0262, FA9550-18-1-0403, and FA9550-19-1-0182. We thank Eric Marineau and the Office of Naval Research for sponsoring the construction and development of the Stevens Shock Tunnel. We also thank AFOSR program manager Sarah Popkin for her support.

References

[1] Holden, M. S., Wadhams, T. P., and MacLean, M. G., "Measurements in Regions of Shock Wave/Turbulent Boundary Layer Interaction from Mach 4 to 10 at Flight Duplicated Velocities to Evaluate and Improve the Models of Turbulence in CFD Codes," Tech. rep., CUBRC, 2014.

[2] Parziale, N. J., Smith, M. S., and Marineau, E. C., "Krypton tagging velocimetry of an underexpanded jet," *Applied Optics*, Vol. 54, No. 16, 2015, pp. 5094–5101. https://doi.org/10.1364/AO.54.005094.

[3] Zahradka, D., Parziale, N. J., Smith, M. S., and Marineau, E. C., "Krypton tagging velocimetry in a turbulent Mach 2.7 boundary layer," *Experiments in Fluids*, Vol. 57, 2016, p. 62. https://doi.org/10.1007/s00348-016-2148-2.

[4] Mustafa, M. A., Hunt, M. B., Parziale, N. J., Smith, M. S., and Marineau, E. C., "Krypton Tagging Velocimetry (KTV) Investigation of Shock-Wave/Turbulent Boundary-Layer Interaction," *Proceedings of AIAA SciTech 2017*, AIAA-2017-0025, Grapevine, Texas, 2017. https://doi.org/10.2514/6.2017-0025.

[5] Mustafa, M. A., , and Parziale, N. J., "Krypton Tagging Velocimetry in the Stevens Shock Tube," *Proceedings of 33rd AIAA Aerodynamic Measurement Technology and Ground Testing Conference*, AIAA-2017-3897, Denver, Colorado, 2017. https://doi.org/10.2514/6.2017-3897.

[6] Mustafa, M. A., Parziale, N. J., Smith, M. S., and Marineau, E. C., "Nonintrusive Freestream Velocity Measurement in a Large-Scale Hypersonic Wind Tunnel," *AIAA Journal*, Vol. 55, No. 10, 2017, pp. 3611–3616. https://doi.org/10.2514/1.J056177.

[7] Mustafa, M. A., Parziale, N. J., Smith, M. S., and Marineau, E. C., "Two-Dimensional Krypton Tagging Velocimetry (KTV-2D) Investigation of Shock-Wave/Turbulent Boundary-Layer Interaction," *Proceedings of AIAA SciTech 2018*, AIAA-2018-1771, Kissimmee, Florida, 2018. https://doi.org/10.2514/6.2018-1771.

[8] Mustafa, M. A., and Parziale, N. J., "Simplified read schemes for krypton tagging velocimetry in N_2 and air," *Optics Letters*, Vol. 43, No. 12, 2018, pp. 2909–2912. https://doi.org/10.1364/OL.43.002909.

[9] Mustafa, M. A., Parziale, N. J., Smith, M. S., and Marineau, E. C., "Amplification and structure of streamwise-velocity fluctuations in compression-corner shock-wave/turbulent boundary-layer interactions," *Journal of Fluid Mechanics*, Vol. 863, 2019, pp. 1091–1122. https://doi.org/10.1017/jfm.2018.1029.

[10] Mustafa, M. A., Shekhtman, D., and Parziale, N. J., "Single-Laser Krypton Tagging Velocimetry Investigation of Supersonic Air and N_2 Boundary-Layer Flows over a Hollow Cylinder in a Shock Tube," *Physical Review Applied*, Vol. 11, No. 6, 2019, p. 064013. https://doi.org/10.1103/PhysRevApplied.11.064013.

[11] Shekhtman, D., Mustafa, M. A., and Parziale, N. J., "Two-photon cross-section calculations for krypton in the 190-220 nm range," *Applied Optics*, Vol. 59, No. 34, 2020, pp. 10826–10837. https://doi.org/10.1364/AO.410806.

[12] Clark, A., McCord, W., and Zhang, Z., "Air Resonance Enhanced Multiphoton Ionization Tagging Velocimetry," *Applied Optics*, Vol. 61, No. 13, 2022, pp. 3748–3753. https://doi.org/10.1364/AO.455216.

[13] Lempert, W. R., Jiang, N., Sethuram, S., and Samimy, M., "Molecular Tagging Velocimetry Measurements in Supersonic Microjets," *AIAA Journal*, Vol. 40, No. 6, 2002, pp. 1065–1070. https://doi.org/10.2514/2.1789.

[14] Lempert, W. R., Boehm, M., Jiang, N., Gimelshein, S., and Levin, D., "Comparison of molecular tagging velocimetry data and direct simulation Monte Carlo simulations in supersonic micro jet flows," *Experiments in Fluids*, Vol. 34, No. 3, 2003, pp. 403–411. https://doi.org/10.1007/s00348-002-0576-7.

[15] Mirzaei, M., Dam, N. J., and van der Water, W., "Molecular tagging velocimetry in turbulence using biacetyl," *Physcial Review E*, Vol. 86, No. 4, 2012, pp. 1–8. https://doi.org/10.1103/PhysRevE.86.046318.

[16] Boedeker, L. R., "Velocity measurement by H_2O photolysis and laser-induced fluorescence of OH," *Optics Letters*, Vol. 14, No. 10, 1989, pp. 473–475. https://doi.org/10.1364/OL.14.000473.

[17] Wehrmeyer, J. A., Ribarov, L. A., Oguss, D. A., and Pitz, R. W., "Flame Flow Tagging Velocimetry with 193-nm H_2O Photodissociation," *Applied Optics*, Vol. 38, No. 33, 1999, pp. 6912–6917. https://doi.org/10.1364/AO.38.006912.

[18] Pitz, R. W., Lahr, M. D., Douglas, Z. W., Wehrmeyer, J. A., Hu, S., Carter, C. D., Hsu, K.-Y., Lum, C., and Koochesfahani, M. M., "Hydroxyl tagging velocimetry in a supersonic flow over a cavity," *Applied Optics*, Vol. 44, No. 31, 2005, pp. 6692–6700. https://doi.org/10.1364/AO.44.006692.

[19] André, M. A., Bardet, P. M., Burns, R. A., and Danehy, P. M., "Characterization of hydroxyl tagging velocimetry for low-speed flows," *Measurement Science and Technology*, Vol. 28, No. 8, 2017, p. 085202. https://doi.org/10.1088/1361-6501/aa7ac8.

[20] McDaniel, J. C., Hiller, B., and Hanson, R. K., "Simultaneous multiple-point velocity measurements using laser-induced iodine fluorescence," *Optics Letters*, Vol. 8, No. 1, 1983, pp. 51–53. https://doi.org/10.1364/OL.8.000051.

[21] Balla, R. J., "Iodine Tagging Velocimetry in a Mach 10 Wake," *AIAA Journal*, Vol. 51, No. 7, 2013, pp. 1–3. https://doi.org/10.2514/1.J052416.

[22] Danehy, P. M., O'Byrne, S., Houwing, A. F. P., Fox, J. S., and Smith, D. R., "Flow-tagging Velocimetry for Hypersonic Flows using Fluorescence of Nitric Oxide," *AIAA Journal*, Vol. 41, No. 2, 2003, pp. 263–271. https://doi.org/10.2514/2.1939.

[23] Michael, J. B., Edwards, M. R., Dogariu, A., and Miles, R. B., "Femtosecond laser electronic excitation tagging for quantitative velocity imaging in air," *Applied Optics*, Vol. 50, No. 26, 2011, pp. 5158–5162. https://doi.org/10.1364/AO.50.005158.

[24] Edwards, M. R., Dogariu, A., and Miles, R. B., "Simultaneous Temperature and Velocity Measurements in Air with Femtosecond Laser Tagging," *AIAA Journal*, Vol. 53, No. 8, 2015, pp. 2280–2288. https://doi.org/10.2514/1.J053685.

[25] Jiang, N., Halls, B. R., Stauffer, H. U., Danehy, P. M., Gord, J. R., and Roy, S., "Selective two-photon absorptive resonance femtosecond-laser electronic-excitation tagging velocimetry," *Optics Letters*, Vol. 41, No. 10, 2016, pp. 2225–2228. https://doi.org/10.1364/OL.41.002225.

[26] Jiang, N., Mance, J. G., Slipchenko, M. N., Felver, J. J., Stauffer, H. U., Yi, T., Danehy, P. M., and Roy, S., "Seedless velocimetry at 100 kHz with picosecond-laser electronic-excitation tagging," *Optics Letters*, Vol. 42, No. 2, 2017, pp. 239–242. https://doi.org/10.1364/OL.42.000239.

[27] Mills, J. L., "Investigation of Multi-Photon Excitation in Argon with Applications in Hypersonic Flow Diagnostics," Ph.D. thesis, Old Dominion University, 2016.

[28] Gragston, M., and Smith, C. D., "10 kHz molecular tagging velocimetry in a Mach 4 air flow with acetone vapor seeding," *Experiments in Fluids*, Vol. 63, No. 85, 2022, pp. 1–9. https://doi.org/10.1007/s00348-022-03438-1.

[29] Andrade, A., Hoffman, E. N., LaLonde, E. J., and Combs, C. S., "Characterization of hydroxyl tagging velocimetry for low-speed flows," *Optics Express*, Vol. 30, No. 23, 2022, pp. 42199–42213. https://doi.org/10.1364/OE.474841.

[30] Lozano, A., "Laser-Excited Luminescent Tracers for Planar Concentration Measurements in Gaseous Jets," Ph.D. thesis, Stanford University, 1992.

[31] Fratantonio, D., Rojas-Cárdenas, M., Mohand, H. S. H., Barrot, C., Baldas, L., and Colin, S., "Molecular tagging velocimetry for confined rarefied gas flows: Phosphorescence emission measurements at low pressure," *Experimental Thermal and Fluid Science*, Vol. 99, 2018, pp. 510–524. https://doi.org/10.1016/j.expthermflusci.2018.08.001.

[32] Tran, T., Kochar, Y., and Seitzman, J., "Measurements of Liquid Acetone Fluorescence and Phosphorescence for Two-Phase Fuel Imaging," *Proceedings of 43rd Aerospace Sciences Meeting and Exhibit*, AIAA-2005-0827, Reno, Nevada, 2005. https://doi.org/10.2514/6.2005-827.

[33] Tran, T. T., "Acetone Planar Laser-Induced Fluorescence and Phosphorescence for Mixing Studies of Multiphase Flows at High Pressure and Temperature," Ph.D. thesis, Georgia Institute of Technology, 2008.

[34] Schulz, C., and Sick, V., "Tracer-LIF diagnostics: quantitative measurement of fuel concentration, temperature and fuel/air ratio in practical combustion systems," *Progress in Energy and Combustion Science*, Vol. 31, 2005, pp. 75–121. https://doi.org/10.1016/j.pecs.2004.08.002.

[35] *ASME B16.5-2009 Pipe Flanges and Flanged Fittings: NPS 1/2 Through NPS 24 Metric/Inch Standard*, ASME, 2009.

[36] *ASME B31.1-2014 Power Piping: ASME Code for Pressure Piping, B31*, ASME, 2014.

[37] Anderson, D. A., Tannehill, J. C., and Pletcher, R. H., *Computational Fluid Mechanics and Heat Transfer*, 1st ed., McGraw-Hill Book Company, 1984.

[38] Shekhtman, D., Hameed, A., Segall, B. A., Dworzanczyk, A. R., and Parziale, N. J., "Initial Shakedown Testing of the Stevens Shock Tunnel," *Proceedings of AIAA SciTech 2022*, AIAA 2022-1402, San Diego, California and Virtual Event, 2022. https://doi.org/10.2514/6.2022-1402.

[39] Goodwin, D. G., "An Open-Source, Extensible Software Suite for CVD Process Simulation," *Proceedings of CVD XVI and EuroCVD Fourteen, M Allendorf, F Maury, and F Teyssandier (Eds.)*, 2003, pp. 155–162.

[40] Browne, S., Ziegler, J., and Shepherd, J. E., "Numerical Solution Methods for Shock and Detonation Jump Conditions," GALCIT - FM2006-006, Caltech, 2006.

[41] Gordon, S., and McBride, B., "Thermodynamic Data to 20000 K for Monatomic Gases," NASA TP-1999-208523, 1999.

[42] McBride, B. J., Zehe, M. J., and Gordon, S., "NASA Glenn Coefficients for Calculating Thermodynamic Properties of Individual Species," NASA TP-2002-211556, 2002.

[43] Sato, K., and Hidaka, Y., "Shock-Tube and Modeling Study of Acetone Pyrolysis and Oxidation," *Combustion and Flame*, Vol. 22, 2000, pp. 291–311. https://doi.org/10.1016/S0010-2180(00)00121-8.

[44] Capelin, B. C., Ingram, G., and Kokolos, J., "The Pyrolytic identification of Organic Molecules: II A Quantitative Evaluation," *Microchemical Journal*, Vol. 19, 1974, pp. 229–252. https://doi.org/10.1016/0026-265X(74)90123-4.

[45] Yu, D., Tian, Z., Wang, Z., Liu, Y., and Zhou, L., "Estimation of Enthalpy of Bio-Oil Vapor and Heat Required for Pyrolysis of Biomass," *Fuel*, Vol. 234, 2018, pp. 1380–1387. https://doi.org/10.1016/j.fuel.2018.08.020.

[46] O'Haver, T., *A Pragmatic Introduction to Signal Processing*, University of Maryland at College Park, 1997.